Combined Effects of Electrostatic and π – π Stacking Interactions: Selective Binding of Nucleotides and Aromatic Carboxylates by Platinum(II) – Aromatic Ligand Complexes

Tatsuo Yajima,[a, b] Giuseppe Maccarrone,[c] Masako Takani,[d] Annalinda Contino,[c] Giuseppe Arena,[c] Reiko Takamido,[b] Mieko Hanaki,[b] Yasuhiro Funahashi,[e] Akira Odani,[f] and Osamu Yamauchi*[a]

Abstract: Adduct formations of Pt^{II} complexes containing an aromatic diimine (DA) and an L-amino acid (A) with an aromatic carboxylate (AR) or a mononucleotide (NMP) has been studied by synthetic, structural, spectroscopic, and calorimetric methods. Several adducts between Pt^{II} complexes, [Pt(DA)(L-A)] (charges are omitted; DA = 2,2′-bipyrimidine (bpm); A = L-arginine (L-Arg), L-alaninate (L-Ala), and AR (= indole-3-acetate (IA), gentisate (GA)) or GMP were isolated as crystals and structurally characterized by the X-ray diffraction method. GMP in [Pt(bpm)(Arg)](GMP)·5H_2O was revealed to be bound through the π – π stacking and guanidinium – phosphate hydrogen bonds. The [Pt(DA)(A)]-AR and -NMP systems in aqueous solution exhibited NMR upfield shifts of the aromatic ring proton signals due to stacking. The stability constants (K) for the adducts were determined by absorption and NMR spectra and calorimetric titrations. The log$K$ values were found to be in the range 1.40 – 2.29 for AR and 1.8 – 3.3 for NMP, the order for NMP being GMP > AMP > CMP > UMP. The ΔH° values were negative for all the systems studied, and the values for AR (= IA and GA) were more negative than those for NMP, indicating that ARs are stronger electron donors than NMPs. Comparison of the log$K$ values for [Pt(bpm)(L-Arg)] and [Pt(bpm)(L-Ala)] (Ala = alaninate) indicated that the Arg moiety further stabilized the adducts by the guanidinium – carboxylate or – phosphate hydrogen bonds. The combined effects of weak interactions on the stability of the adducts in solution are discussed on the basis of the thermodynamic parameters and solid state structures.

Keywords: hydrogen bonds · nucleotides · platinum(II) complexes · stability constants · stacking interactions

Introduction

Specificity and efficiency of chemical and biological reactions owe much to noncovalent or weak interactions.[1] These are important for the stabilization of for example protein structures,[1c, 2–5] DNA base pair formation,[6] electron transfer pathway formation,[7] and are responsible not only for recognition and specific binding between molecules but also for the structural change upon binding.[1b, d] Various interactions including CH – π,[8] NH – π,[9] and cation – π[10–13] interactions are thus attracting much attention. Molecules can be organized by metal coordination and various weak interactions, so that the molecular design and effective use of such binding forces are of prime importance in supramolecular chemistry.[14] Highly specific intermolecular binding as observed for proteins is attained by combination of several interacting groups, so that information on the modes and contributions of the interactions of individual groups[15] will serve as a basis for organization of molecules and construction

[a] Prof. O. Yamauchi, T. Yajima
Faculty of Engineering, Kansai University
Suita, Osaka 564-8680 (Japan)
Fax: (+81) 6-6330-3770
E-mail: osamuy@ipcku.kansai-u.ac.jp

[b] T. Yajima, R. Takamido, M. Hanaki
Department of Chemistry, Graduate School of Science
Nagoya University, Nagoya 464-8602 (Japan)

[c] Dr. G. Maccarrone, Dr. A. Contino, Prof. G. Arena
Dipartimento di Scienze Chimiche
Universitá degli Studi di Catania
95125 Catania (Italy)

[d] Dr. M. Takani
Faculty of Pharmaceutical Sciences, Kanazawa University
Kanazawa 920-1192 (Japan)

[e] Dr. Y. Funahashi
Nagoya Institute of Technology
Nagoya 466-8555 (Japan)

[f] Dr. A. Odani
Research Center for Materials Science, Nagoya University
Nagoya 464-8602 (Japan)

 DOI: 10.1002/chem.200304728

of multicomponent reaction systems. Planar platinum(II) complexes with aromatic nitrogen ligands are known to be DNA intercalators,[16–18] while chiral octahedral complexes of ruthenium(II) and other metal ions with similar ligands have been shown to bind with DNA in an enantioselective way.[19–23] In dilute aqueous solution Pt^{II} complexes such as $[Pt(phen)(en)]^{2+}$ (phen = 1,10-phenanthroline; en = ethylenediamine)[24] were found to form stable adducts with nucleotide 5′-monophosphates (NMPs) through aromatic ring stacking as an important binding force.[25–29] This result supported the DNA intercalation of Pt^{II} complexes by stacking and was in line with the X-ray crystal structure analyses, for example, of [PtCl(terpy)]·AMP[30] and [Pt(bpy)(en)]·AMP[31] (terpy = 2,2′:6′,2″-terpyridine) and extended Hückel molecular orbital calculations.[26]

Intramolecular electrostatic interactions or hydrogen bonds and stacking interactions in mixed ligand metal complexes involving amino acids have been shown to enhance the stability of the complexes relative to those without such interactions.[31–37] These observations indicate that metal complexes of ligands with interacting groups can be the site of recognition and may be regarded as receptors for uncoordinated molecules. In addition the metal center such as Pt^{II} is expected to assist the interactions by its planar coordination structure and electron withdrawing effect.[28] With these points in mind, we carried out synthetic, structural, spectral, and calorimetric studies on the receptor ability of Pt^{II} complexes incorporating an aromatic bidentate ligand (DA) and an amino acid (L-A) with a charged or polar side chain group, [Pt(DA)(L-A)] (charges are omitted). In the present studies we aimed at obtaining information on the combined effects of stacking and electrostatic interactions in selective adduct formation with NMPs or aromatic carboxylates (ARs) as guest molecules (Scheme 1). NMPs such as AMP and GMP have now been found to be bound more strongly with [Pt(DA)(A)] having a basic amino acid, L-Arg or L-Lys, than with the complexes having L-Ala in place of L-Arg or L-Lys. The [Pt(bpm)(L-Arg)]–GMP adduct isolated as crystals has been revealed to have intramolecular guanidinium–phosphate hydrogen bonds and bpm–guanine $\pi-\pi$ interactions and interesting guanine–guanine hydrogen bonds, as revealed for the guanine quartet in telomeres, between the adduct units. These results substantiate the effects of combined weak interactions and correlate the structural and solution chemical phenomena.

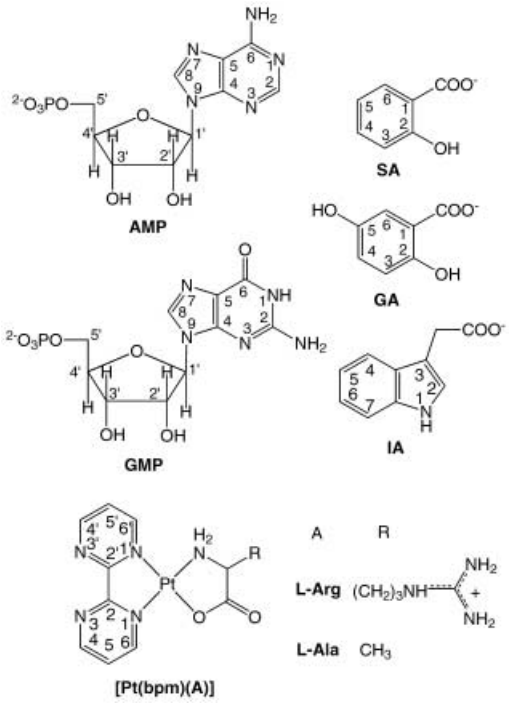

Scheme 1. Structures, numbering schemes, and abbreviations of selected ligands and complexes used.

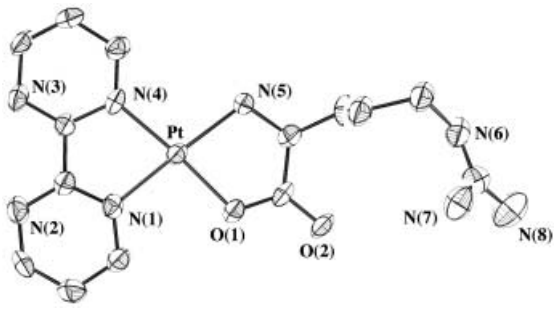

Figure 1. ORTEP drawing of [Pt(bpm)(L-Arg)]·Cl_2·$3H_2O$ (**2**) with the atomic labeling scheme. Thermal ellipsoids are drawn at the 50% probability level. Chloride ions and water molecules are omitted for clarity. Selected bond lengths [Å] and bond angles [°]: Pt–O(1) 1.993(7), Pt–N(1) 2.041(10), Pt–N(4) 1.996(8), Pt–N(5) 2.062(10); ∢O(1)-Pt-N(1) 95.6(4), ∢O(1)-Pt-N(4) 175.4(3), ∢O(1)-Pt-N(5) 82.1(4), ∢N(1)-Pt-N(4) 79.8(4), ∢N(1)-Pt-N(5) 177.1(4), ∢N(4)-Pt-N(5) 102.5(4).

Results and Discussion

Structural characterization of Pt^{II} complexes and the adducts with guest molecules

Molecular structure of [Pt(bpm)(L-Arg)]Cl_2·$3H_2O$ (2): The structure of complex **2**, one of the Pt^{II} complexes with a positively charged side chain, was determined by the X-ray diffraction method and is shown in Figure 1; Pt^{II} is in a square-planar geometry formed by the two nitrogen atoms from bpm and a nitrogen and an oxygen atom from L-Arg. The angle between the bpm plane and the plane formed by the Pt^{II}–L-Arg bonds is 1.8°, which indicates that the Pt^{II} coordination plane is nearly planar. The Pt–N bond lengths (2.041(10), 1.996(8), and 2.062(10) Å for Pt–N(1), Pt–N(4), and Pt–N(5), respectively) and the Pt–O bond length (1.993(7) Å) are within the ranges of the reported values.[38] The side chain containing the guanidinium group is extended sideways from the coordination plane and the N(6)–H moiety is involved in the hydrogen bond with a chloride ion with the N(6)–Cl(2) distance of 3.30(1) Å.

Structures of the adducts and interaction modes: The reactions of IA with **1** and **2** gave the adducts **3** and **4**, respectively, and the structure of **3** was successfully determined. On the other hand, **1** and **2** gave adducts **6** and **5**,

respectively, with GA; **5** was structurally characterized. Complex **2** reacted with GMP to give the adduct **7** as crystals, whose structure has been found to consist of discrete adduct units bound by hydrogen bonds in the crystal structure.

[Pt(bpm)(L-Ala)](IA)·7H$_2$O (3): The structure of **3** depicted in Figure 2 shows that the [Pt(bpm)(L-Ala)] moiety has a planar coordination structure with the bond lengths around the Pt^{II} center nearly the same as those for **2**. The IA molecule is bound in parallel with the coordination plane through stacking with coordinated bpm with the spacing of ca. 3.4 Å (N(1)–C(17) 3.35(2), C(4)–C(18) 3.35(1), and N(4)–C(19) 3.46(1) Å). Interestingly, one of the carboxylate oxygen atoms (O(3)) of IA is hydrogen-bonded to the coordinated amino group with the O(3)–N(5) distance of 2.94 Å, and this may have affected the orientation of IA above the coordination plane. The carboxylate oxygen atoms are further bound with the neighboring water molecules with the distances of 2.70–2.75 Å. The crystal structure is constructed by the piles of the adduct units, forming a layer structure with alternating stacks of the bpm and indole rings (N(4)–C(13′) 3.39(1) and N(3)–C(12′) 3.45(2) Å) (Figure 3). The neighboring piles are connected by the IA carboxylate–water molecule hydrogen bonds.

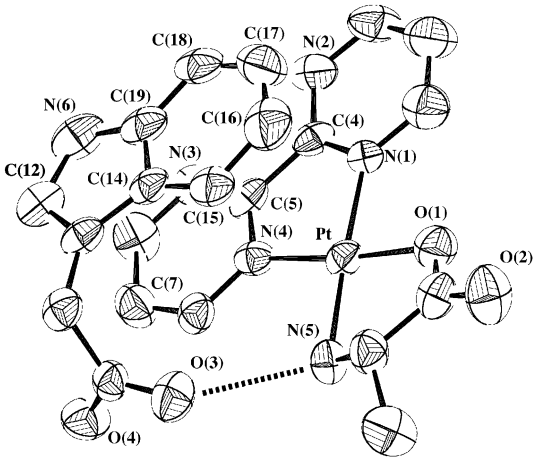

Figure 2. ORTEP drawing of [Pt(bpm)(L-Ala)](IA)·7H$_2$O (**3**) with the atomic labeling scheme. Thermal ellipsoids are drawn at the 50% probability level. Water molecules are omitted for clarity. Selected bond lengths [Å] and bond angles [°]: Pt–O(1) 1.994(7), Pt–N(1) 2.009(8), Pt–N(4) 1.982(8), Pt–N(5) 2.051(8); ∢O(1)-Pt-N(1) 95.3(3), ∢O(1)-Pt-N(4) 174.3(3), ∢O(1)-Pt-N(5) 82.0(3), ∢N(1)-Pt-N(4) 79.4(3), ∢N(1)-Pt-N(5) 177.1(3), ∢N(4)-Pt-N(5) 103.3(3). Selected interatomic distances [Å]: Pt···C(16) 3.52(1), O(3)···N(5) 2.94(1), N(1)···C(17) 3.35(2), N(4)···C(19) 3.46(1), C(4)···C(18) 3.35(1), C(7)···C(12) 3.47(2).

[Pt(bpm)(L-Arg)](GA)Cl·2H$_2$O (5): The structure of **5** shown in Figure 4 indicates that the adduct exists in two forms in a unit cell which may be regarded as a dimer. The two

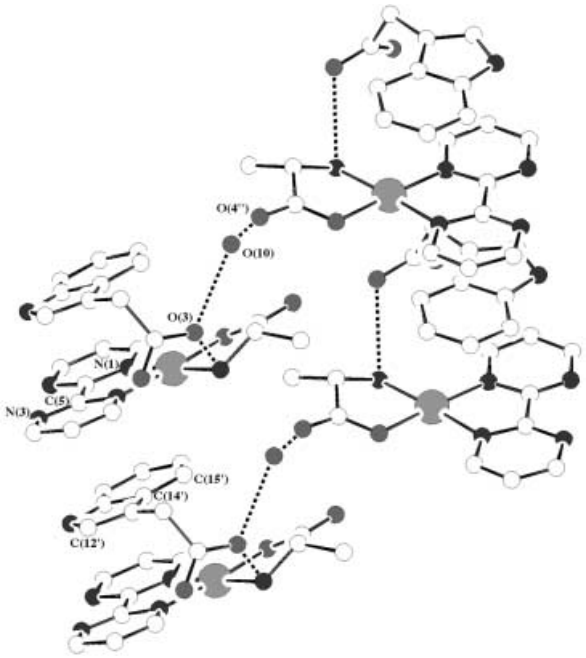

Figure 3. Hydrogen-bonding network showing intermolecular association of **3**. Selected interatomic distances [Å]: Pt···C(15′) 3.49(1), O(3)···O(10) 3.40(1), O(4″)···O(10) 2.70(1), N(1)···C(15′) 3.48(1), N(3)···C(12′) 3.45(2), C(5)···C(14′) 3.48(1).

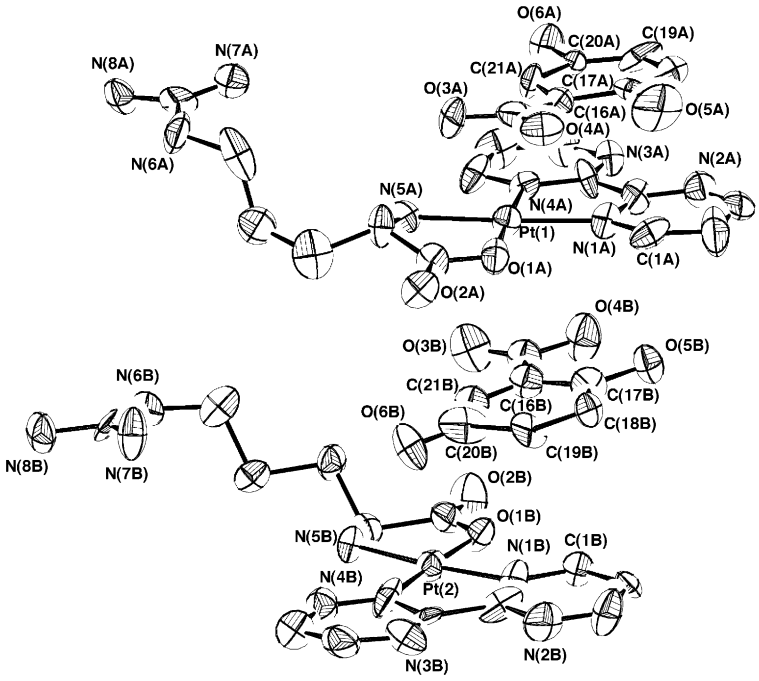

Figure 4. ORTEP drawing of [Pt(bpm)(L-Arg)]$_2$(GA)$_2$·Cl$_2$·4H$_2$O (**5**) with the atomic labeling scheme. Thermal ellipsoids are drawn at the 50% probability level. Chloride ions and water molecules are omitted for clarity.

complex molecules appear to sandwich a GA molecule with the same side of the coordination plane facing GA, and the remaining GA molecule stacks with a complex on the opposite side. The aromatic ring of GA is bound with bpm above one of the coordinated nitrogen atoms with the face-to-face distance of 3.3 Å (O(6A)–N(4A) 3.20(3), N(1A)–C(20A) 3.32(3), O(6B)–N(4B) 3.24(3), and N(1B)–C(20B) 3.39(4) Å) (Table 1). The side chain guanidinium group of Arg is stretched outward to be involved in hydrogen bonds, while the carboxylate group of GA is oriented in a different direction. The other GA molecule of the dimeric unit is close to the complexes sandwiching GA to be also bound through face-to-face stacking. The GA carboxylate oxygen atoms of each adduct unit are bound with the Arg guanidinium group of a neighboring unit through two parallel O···H–N hydrogen bonds with the O–N distances of 2.89(3) (O(3A)–N(7A′)), 2.84(3) (O(4A)–N(8A′)), and 2.80(3) Å (O(3B)–N(7B″) and O(4B)–N(8B″)) (Figure 5). These hydrogen bonds contribute to the formation of the crystal structure. In dilute aqueous solution, however, these intermolecular hydrogen bonds should be ineffective, and instead the hydrogen bonds between the guanidinium and GA carboxylate groups within the same Pt^{II} complex–GA adduct unit should become important for the adduct stability (see below).

Table 1. Selected bond lengths, angles, and interatomic distances for $[Pt(bpm)(L\text{-}Arg)]_2(GA)_2 \cdot Cl_2 \cdot 4H_2O$ (**5**).

a) Bond lengths [Å]			
Pt(1)–O(1A)	2.03(2)	Pt(1)–N(1A)	1.97(2)
Pt(1)–N(4A)	2.04(2)	Pt(1)–N(5A)	2.03(2)
Pt(2)–O(1B)	1.95(2)	Pt(2)–N(1B)	2.04(2)
Pt(2)–N(4B)	1.92(3)	Pt(2)–N(5B)	2.00(2)

b) Bond angles [°]			
O(1A)-Pt(1)-N(1A)	96.6(7)	O(1A)-Pt(1)-N(4A)	176.5(6)
O(1A)-Pt(1)-N(5A)	83.8(7)	N(1A)-Pt(1)-N(4A)	80.0(7)
N(1A)-Pt(1)-N(5A)	177.9(8)	N(4A)-Pt(1)-N(5A)	99.6(8)
O(1B)-Pt(2)-N(1B)	96.2(7)	O(1B)-Pt(2)-N(4B)	177.1(7)
O(1B)-Pt(2)-N(5B)	82.6(7)	N(1B)-Pt(2)-N(4B)	81.0(8)
N(1B)-Pt(2)-N(5B)	176.3(8)	N(4B)-Pt(2)-N(5B)	100.2(7)

c) Interatomic distances [Å]					
Pt(1)	C(21A)	3.39(3)	Pt(1)	C(16B‴)	3.39(3)
Pt(2)	C(16A⁗)	3.43(2)	Pt(2)	C(21B)	3.45(2)
O(3A)	N(7A′)	2.89(3)	O(4A)	N(8A′)	2.84(3)
O(6A)	N(4A)	3.20(3)	O(3B)	N(7B″)	2.80(3)
O(4B)	N(8B″)	2.80(3)	O(6B)	N(4B)	3.24(3)
N(1A)	C(20A)	3.32(3)	N(1A)	C(17B‴)	3.33(3)
N(1A)	C(19A)	3.49(3)	N(1B)	C(17A⁗)	3.35(3)
N(1B)	C(20B)	3.39(4)	N(1B)	C(19B)	3.44(3)
C(1A)	C(19A)	3.51(3)	C(1B)	C(18B)	3.51(4)

[Pt(bpm)(L-Arg)](GMP) · 5H₂O (7): The structure of **7** (Figure 6) indicates that the guanine ring of GMP is in a face-to-face stacking arrangement with a bpm-GMP distance of 3.3 Å (N(13)–C(5) 3.29(2) Å), which may be compared with that in [Pt(bpy)(en)](AMP)[31] and [Pt(terpy)Cl](AMPH),[30] with the distances of 3.5 and 3.3 Å, respectively. The side chain of L-Arg is stretched along with the ribose 5′-phosphate moiety of GMP toward to the opposite side of the stacked coordination plane to interact with the phosphate moiety via two parallel hydrogen bonds (N(6)–O(8) 2.79(2), N(7)–O(9) 2.83(1) Å). The hydrogen bond with the coordinated amino group (N(5)–O(8) 2.93(2) Å) further contributes to fixing the phosphate group. It is remarkable that one [Pt(bpm)(L-Arg)] complex molecule interacts with a GMP molecule via combination of the stacking interaction and hydrogen bonds to form a nearly discrete adduct unit even in the crystal structure, where the adduct units are arranged in zigzag lines by unique guanine–guanine hydrogen bonds (N(9′)–N(13) 2.82(2) and O(3)–N(10′) 2.86(2) Å) (Figure 7). The guanine–guanine pairing pattern is reminiscent of that in the guanine quartet in telomeres[39, 40] and indicates a versatile

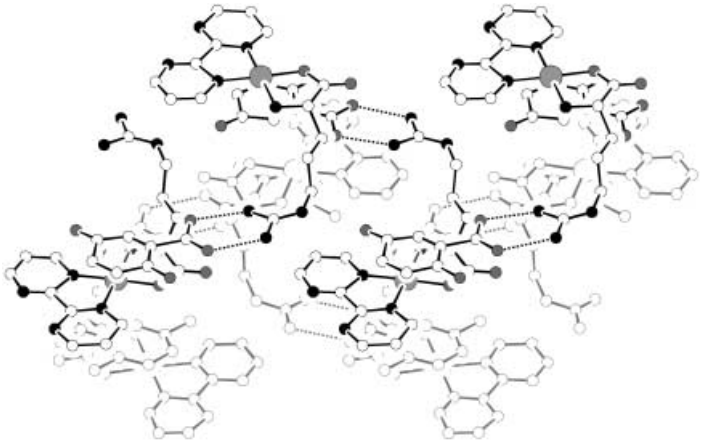

Figure 5. Hydrogen-bonding network showing intermolecular association of **5**.

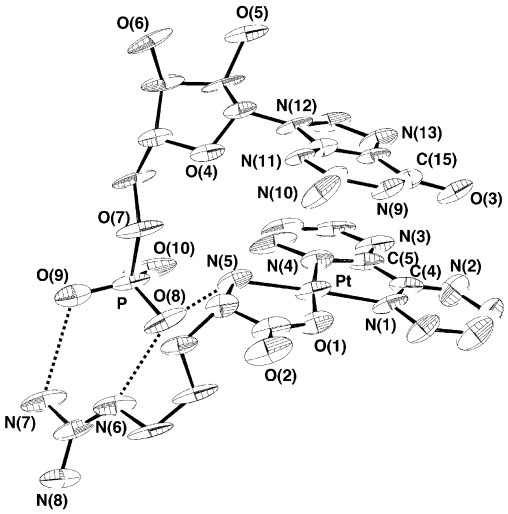

Figure 6. ORTEP drawing of $[Pt(bpm)(L\text{-}Arg)](GMP) \cdot 5H_2O$ (**7**) with the atomic labeling scheme. Thermal ellipsoids are drawn at the 50% probability level. Water molecules are omitted for clarity. Selected bond lengths [Å] and bond angles [°]: Pt–O(1) 1.99(1), Pt–N(1) 2.04(1), Pt–N(4) 2.04(1), Pt–N(5) 2.06(1); ∢O(1)-Pt-N(1) 95.7(4), ∢O(1)-Pt-N(4) 174.8(5), ∢O(1)-Pt-N(5) 82.9(4), ∢N(1)-Pt-N(4) 79.2(5), ∢N(1)-Pt-N(5) 177.4(5), ∢N(4)-Pt-N(5) 102.2(5). Selected interatomic distances [Å]: O(3)···N(1) 3.45(2), O(3)···C(4) 3.48(2), O(8)···N(5) 2.93(2), O(8)···N(6) 2.79(2), O(9)···N(7) 2.83(1), N(1)···C(15) 3.44(2), N(4)···N(13) 3.46(2), N(13)···C(5) 3.29(2).

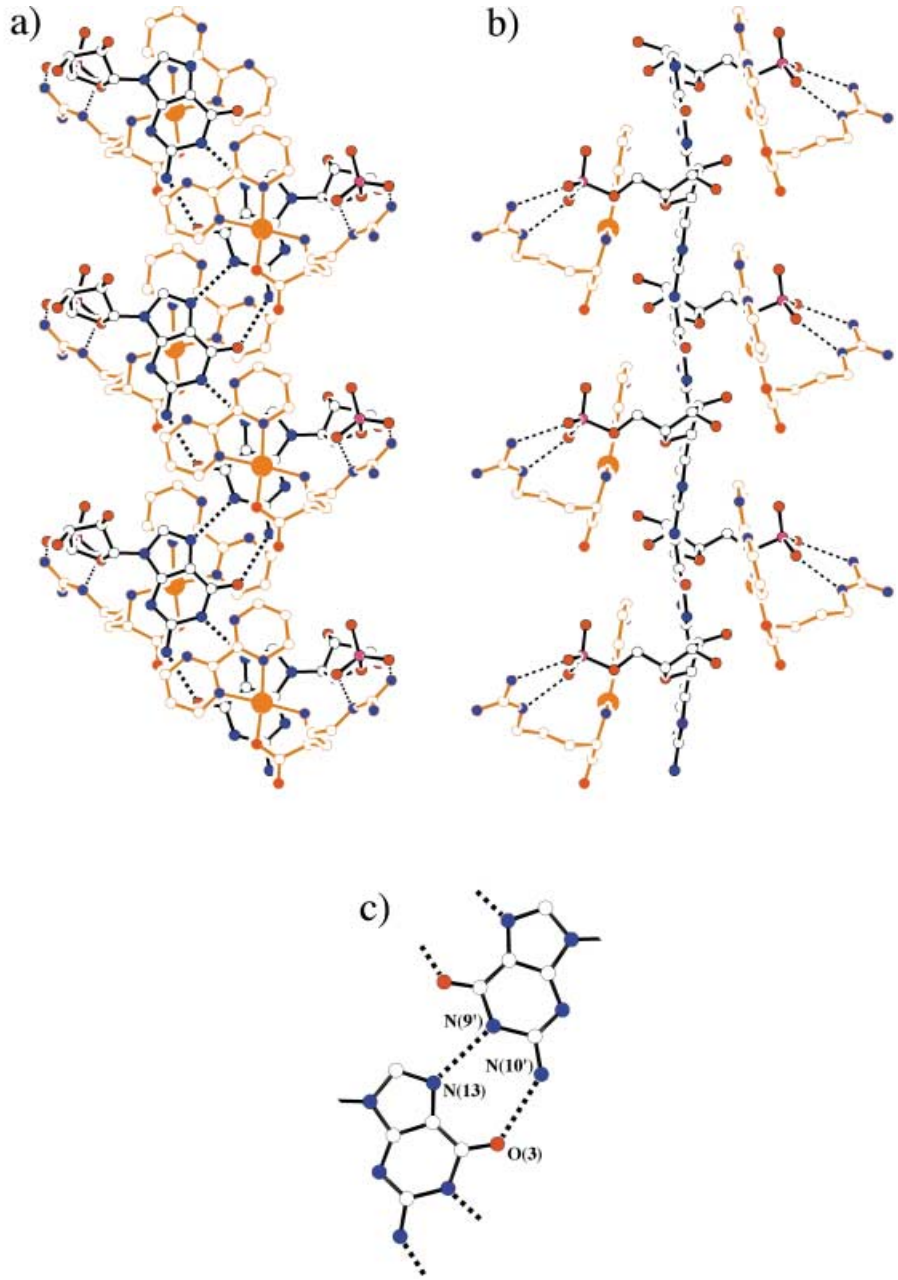

Figure 7. Intramolecular guanidinium–phosphate and intermolecular guanine–guanine hydrogen bonds for **7**; a) top view, b) side view, and c) interactions between guanines. Selected interatomic distances [Å]: O(3)···N(10′) 2.86(2), N(9′)···N(13) 2.82(2).

hydrogen-bonding ability of the guanine base. The zigzag lines are connected by the interactions between the phosphate and sugar hydroxyl groups of two neighboring GMP molecules with the O(6)–O(8″) distance of 2.72(1) Å.

Adduct formation with aromatic carboxylates

We reported previously that Pt^{II} complexes containing for example bpy, phen, formed adducts with nucleotides such as AMP, GMP, and NAD.[25–29] The solid state structures of **3** (Figure 2) and **5** (Figure 4) indicate that **1**, **2**, and probably other Pt^{II} complexes have the ability to form adducts with the aromatic carboxylates through aromatic ring stacking and hydrogen bonding.

^{1}H NMR spectra and stability constants: The ^{1}H NMR spectra of the Pt^{II} complex–AR systems (AR = IA, SA, or GA) in D_2O, measured at room temperature for solutions containing 2 mM AR and varying amounts (0–10 mM) of **1** or **2**, indicated that the signals for the aromatic protons of AR are shifted upfield upon formation of adducts due to the ring current effect,[41, 42] while the shifts due to self-stacking in AR solutions (<10 mM) were found to be smaller than 0.01 ppm. The upfield shift $\Delta\delta$, which is expressed as the difference between the shift of AR (δ_{AR}) and that in the presence of a Pt^{II} complex ($\delta_{Pt\text{-}AR}$), $\delta_{AR} - \delta_{Pt\text{-}AR}$, reflects the mode and extent of stacking interactions. Figure 8 illustrates the concentration dependencies of the $\Delta\delta$ values for the indole protons in the **2**–IA system, which indicates the increase of $\Delta\delta$ values with the concentration of the complex and support that the indole ring of IA is stacked with the bpm moiety of **2** in dilute solution. Similar curves were obtained for the **1**–IA system. The observed shifts for 10 mM Pt^{II} complex are large for H7 and H6 ($\Delta\delta = 0.41 - 0.47$ ppm for **2** and 0.34–0.39 ppm for **1**) and small for H2 and H4 ($\Delta\delta =$ 0.22–0.33 ppm for **2** and 0.20–0.31 ppm for **1**). This may reflect a rather restricted orientation of IA above the Pt^{II} coordination plane due to the hydrogen bond as revealed for **3** in the solid state. On the other hand, the upfield shifts for SA ($\Delta\delta = 0.21 - 0.28$ ppm for **2** and 0.18–0.24 ppm for **1**) and GA ($\Delta\delta = 0.34 - 0.40$ ppm for **2** and 0.30–0.34 ppm for **1**) are similar for all the protons, probably because the benzene ring is smaller than the indole ring. Since the carboxylate group is coplanar with the benzene ring, it should affect the orientation because of the repulsion between this and the coordinated carboxylate group in **1** and **2**. The effect of the guanidinium group is evident from the larger $\Delta\delta$ values for **2** as compared with those for **1**, and suggests that electrostatic interactions or hydrogen bonds between the Pt^{II} complexes and AR contribute to stabilization

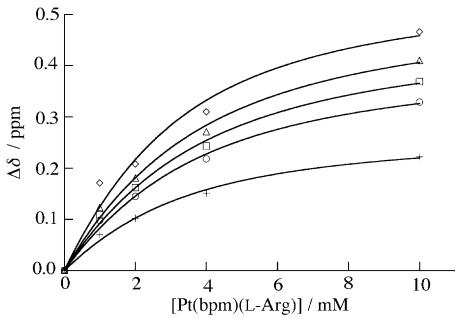

Figure 8. Upfield shifts of IA in [Pt(bpm)(L-Arg)] – IA (in D_2O) plotted against concentrations of the Pt^{II} complex. The curves were fitted by the least-squares treatment. [IA] = 2 mM; 23 °C; I = var. + IA2, ○ IA 4, □ IA 5, △ IA6, ◇ IA7.

of the adduct formed. The adduct formation is expressed by Equation (1) for the 1:1 species (charges are omitted for clarity):

$$[\mathrm{Pt(bpm)(A)}] + \mathrm{AR} \overset{K}{\rightleftharpoons} [\mathrm{Pt(bpm)(A)}]\cdots\mathrm{AR} \quad (1)$$

where A refers to L-Arg or L-Ala and AR to IA, SA, or GA. The stability constants K have been determined by a least-squares curve fitting procedure using the $\Delta\delta$ values for H5 for IA, H4 for SA, and H3 for GA, obtained at 23 °C (I = var.). The $\log K$ values together with the calculated $\Delta\delta$ values ($\Delta\delta_{calcd}$) for completely stacked species are shown in Table 2,

Table 2. Stability constants, $\log K$, for Pt^{II} complex – AR adducts and upfield shifts, $\Delta\delta_{calcd}$, for completely stacked species calculated from the chemical shifts of ^{1}H NMR spectra at room temperature.[a]

	[Pt(bpm)(L-Arg)]$^{2+}$ (**2**)			[Pt(bpm)(L-Ala)]$^{+}$ (**1**)		
	$\log K$	$\Delta\delta_{calcd}$ [ppm]	proton	$\log K$	$\Delta\delta_{calcd}$ [ppm]	proton
IA	2.29(1)	0.52(1)	H5	1.84(2)	0.71(1)	H5
GA	2.20(6)	0.66(3)	H3	1.84(5)	0.89(6)	H3
SA	2.02(7)	0.44(3)	H4	1.40(3)	0.96(5)	H4

[a] Values in parentheses denote estimated standard deviations.

which indicates that the $\log K$ values are in the range 1.40 – 2.29 and that the adducts with **2** are more stable than those with **1** by about 0.4 – 0.6 log units. This stability difference is most probably due to the hydrogen bonds by the guanidinium group of **2** which may contribute to binding and fixing the AR molecule close to the coordination site. IA forms the most stable adducts because of its aromatic ring size and high electron density, and the stability difference between GA and SA is ascribed to the effect of an additional hydroxyl group in GA increasing the electron density of the benzene ring. The [Pt(bpm)(A)]···AR adducts were found to be somewhat less stable than the corresponding adducts with NMP (see below).

^{195}Pt NMR spectra: Addition of AR to an aqueous solution (20 mM) of **2** caused a downfield shift of the ^{195}Pt signal relative to the shift of $[Pt(en)_2]Cl_2$ as standard. The AR concentration dependencies of the ^{195}Pt downfield shifts ($\Delta\delta_{Pt}$) for the **2** – AR systems are shown in Table 3, which indicates that the electron density of the Pt^{II} center was decreased upon adduct formation with AR. The downfield

Table 3. Downfield shifts ($\Delta\delta_{Pt}$ [ppm]) for ^{195}Pt NMR of [Pt(bpm)(L-Arg)] – AR systems.[a]

[AR] [mM]	IA	GA	SA
10	18.4	10.5	8.6
20	32.4	20.7	12.2
40	54.8	35.9	24.8
60	68.0	42.0	32.1
100	73.1	47.1	38.2
200	82.3	54.3	41.6

[a] The shifts are expressed relative to the shift of $[Pt(en)_2]Cl_2$.

shifts for 100 % adduct formation ($\Delta\delta_{Pt,adduct}$) were calculated from the $\log K$ values to be 115(5), 75(1), and 59(2) ppm for IA, GA, and SA, respectively, which implies that the electronic effect on Pt^{II} is greater for more stable or more strongly stacked adducts. These findings are in line with our previous observations[28] for the Pt^{II} complex – NMP systems where the ^{195}Pt NMR downfield shifts were attributed to electron density decrease due to stacking interactions as a result of delocalization of the electrons of Pt^{II} over coordinated and stacked aromatic rings; we also observed a linear relationship between the $\Delta\delta_{Pt}$ values and the enthalpy changes ($-\Delta H^\circ$) for the adduct formation with NMP and interpreted the results as reflecting the bonding interaction between the aromatic rings with charge transfer from the π-orbital (next HOMO) of NMP to the π* orbital (LUMO) of [Pt(bpy)(en)].[26] The $\log K$ and $\Delta\delta_{Pt,adduct}$ values obtained by the present studies support that stacking as seen in the solid state structures is the principal force for the adduct formation in solution.

Adduct formation with NMP

^{1}H NMR spectra: The ^{1}H NMR chemical shifts for **1**, **2**, and AMP in D_2O are summarized in Table 4, and the numbering schemes for bpm and AMP are shown in Scheme 1. The assignment has been made by comparing the spectra for [Pt(bpm)(en)] (**9**) and [Pt(bpm)(Gly)] (**8**). The spectra for 1:1 **1** – and **2** – AMP systems exhibited upfield shifts, $\Delta\delta = \delta_{[Pt(bpm)(A)]} - \delta_{adduct}$ and $\delta_{NMP} - \delta_{adduct}$, for the signals of both bpm and AMP, respectively, resulting from adduct formation. The $\Delta\delta$ values for the 1:1 **2** – AMP system (10 mM) were 0.18 ppm for H6 of bpm and 0.21 ppm for H8 of AMP. Since the upfield shift for H8 of AMP due to self-stacking was about 0.1 ppm for 10 mM AMP, the observed upfield shifts support that the Pt^{II} complexes form adducts through stacking

Table 4. ^{1}H NMR upfield shifts ($\Delta\delta$ [ppm]) for 1:1 Pt^{II} complex – AMP systems.

		[Pt(bpm)(L-Arg)] (**2**)		[Pt(bpm)(L-Ala)] (**1**)	
	proton	5 [mM]	10 [mM]	5 [mM]	10 [mM]
bpm	H4	0.007	0.009	0.008	0.011
	H4′	0.015	0.017	0.008	0.012
	H5	0.004	0.006	0.007	0.010
	H5′	– 0.036	– 0.038	– 0.019	– 0.025
	H6	0.153	0.176	0.080	0.113
	H6′	0.042	0.056	0.028	0.039
AMP	H8	0.179	0.207	0.078	0.115
	H2	0.142	0.171	0.084	0.123
	H1′	0.089	0.106	0.049	0.071

between the bpm and adenine rings. The $\Delta\delta$ values for the bpm protons of **1** and **2** plotted against the concentration of AMP show that the H6 signal exhibited the largest upfield shift ($\Delta\delta$ = ca. 0.4 ppm at 100-fold excess of AMP). The H6′ signal also shifted upfield ($\Delta\delta$ = ca. 0.1 ppm), but the other signals were rather insensitive to the adduct formation ($\Delta\delta <$ 0.1 ppm). The $\Delta\delta$ values for H6 and H6′ protons were larger for **2** than for **1**, probably reflecting the adduct stability.

Stability constants calculated from the absorption spectral changes: The absorption spectra of various Pt^{II} complex–NMP systems showed changes in the 300–450 nm region corresponding to the charge transfer between the stacked aromatic rings. Figure 9 illustrates the difference absorption

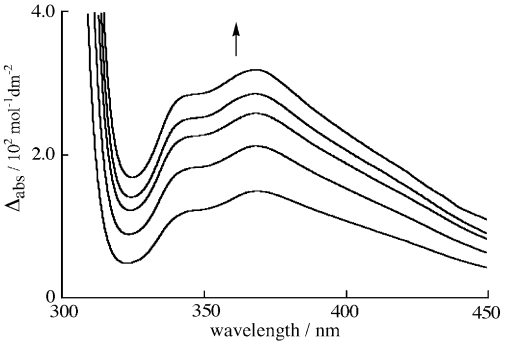

Figure 9. Difference absorption spectra of 1:*n* [Pt(bpm)(en)]–GMP systems ([Pt(bpm)(en)], 0.1 mM; $n = 10-50$; I = var.).

spectra measured for the 1:n [Pt(bpm)(en)]–GMP systems ($n = 0-50$) in aqueous solution (I = var.). Various spectral patterns were observed for [Pt(DA)(en or A)]–NMP systems (DA = bpm, bpy, phen, and dpa; A = L-Ala, L-Arg, and L-Lys). The stability constant K for the adduct formation [Eq. (2)], which is similar to Equation (1), can be calculated by a nonlinear least-squares method by using the intensities of the difference spectra (Δ_{abs}) at the wavelength showing the largest spectral changes:

$$[Pt(DA)(en\ or\ A)] + NMP \overset{K}{\rightleftharpoons} [Pt(DA)(en\ or\ A)]\cdots NMR \qquad (2)$$

Exclusive formation of the 1:1 adduct was confirmed by the Benesi–Hildebrand plots giving linear relationships. The $\log K$ values for the [Pt(DA)(en or A)]···NMP systems (NMP = AMP, GMP, CMP, and UMP) determined at pH 6.5–8.5 (23 °C; I = var.) are summarized in Table 5, which shows that the stability sequence viewed from the nucleobases is in the order, GMP ≥ AMP > CMP ≃ UMP for [Pt(bpy)(en or A)], in agreement with our previous results.[25–29] The stability of the adducts decreased in the order of DA, phen > bpy > dpa > bpm; this indicates that phen, which has the largest aromatic ring forms the most stable adducts due to effective aromatic ring stacking and that bpy with a conjugated π-system interacts with NMP more effectively than dpa without it. The adducts with the bpm-containing Pt^{II} complexes are less stable than those containing phen and bpy by 0.3–0.7 log units. The charged side chain of A has a strong effect on the stability of the adducts. The [Pt(DA)(A)]···NMP adducts

Table 5. Stability constants, $\log K$, for Pt^{II} complex–NMP adducts calculated from absorption spectra at pH 6.5–8.5 (23 °C; I = var.).[a]

Complex	AMP	GMP	CMP	UMP	Ado
[Pt(bpy)(en)]$^{2+}$	2.79(4)	2.85(3)	2.36(4)	1.9(1)	
[Pt(bpy)(L-Arg)]$^{2+}$ (**10**)	3.13(3)	3.3(2)	2.37(5)	2.2(1)	2.11(8)
[Pt(bpy)(L-Lys)]$^{2+}$ (**11**)	3.06(2)	3.23(4)	2.25(4)	2.38(7)	2.09(5)
[Pt(bpy)(L-Asn)]$^{+}$	2.43(4)	2.54(1)	1.84(8)	1.8(2)	1.8(3)
[Pt(bpy)(L-Gln)]$^{+}$	2.62(4)	2.87(8)	1.89(6)	1.98(9)	2.27(2)
[Pt(bpy)(L-Ala)]$^{+}$ (**12**)	2.56(2)	2.75(7)	1.9(1)	1.8(2)	1.82(4)
[Pt(bpy)(Gly)]$^{+}$	2.42(1)	2.70(5)	1.9(1)	1.64(5)	1.72(8)
[Pt(phen)(en)]$^{2+}$	3.09(3)	3.01(3)			
[Pt(phen)(L-Arg)]$^{2+}$	3.23(5)	3.22(5)			2.00(4)
[Pt(phen)(L-Lys)]$^{2+}$	3.12(3)	3.19(6)			2.03(4)
[Pt(phen)(L-Ala)]$^{+}$	2.72(2)	2.68(2)			1.98(6)
[Pt(dpa)(en)]$^{2+}$ (**13**)	2.58(2)	2.45(5)			
[Pt(bpm)(en)]$^{2+}$ (**9**)	2.39(4)	2.39(5)			
[Pt(bpm)(L-Arg)]$^{2+}$ (**2**)	2.80(2)	2.96(4)			
[Pt(bpm)(L-Ala)]$^{+}$ (**1**)	2.14(2)	2.12(4)			

[a] Values in parentheses denote estimated standard deviations.

(DA = bpy, phen, and bpm; A = L-Arg and L-Lys; NMP = AMP and GMP) are more stable than the [Pt(DA)(L-Ala)]···NMP adducts by 0.4–0.8 log units, suggesting that the positively charged guanidinium and ammonium groups of L-Arg and L-Lys, respectively, contribute to the adduct stability by interaction with the negatively charged phosphate group of NMP. This is supported by the fact that the stability constants for Ado, which has no phosphate group are very similar to each other irrespective of amino acids in the Pt^{II} complexes. Comparison of the present $\log K$ values for [Pt(DA)(en)] (DA = phen and bpy) with those determined at I = 0.1 M (KNO_3) reveals that there is a decrease of ca. 0.5 log unit due to addition of KNO_3.[27, 28] The difference is considered to correspond to the contribution of the electrostatic interactions of the phosphate group with the Pt center and the amino group of en.

Thermodynamic aspects of adduct formation

Calorimetric studies: The $\log K$ values as well as the associated enthalpy and entropy values for formation of the adducts between the complexes (**1**, **2**, **9**, and **13**) and ARs (IA and GA) or NMPs (AMP and GMP) were determined by calorimetry (Table 6). It is worth mentioning that the stability constants for NMP determined by calorimetric measurements are in good agreement with those obtained by spectroscopy (see above); the $\log K$ values obtained through the two techniques, which probe different physical parameters, are coincident within the experimental error. The discrepancy observed for [Pt(bpm)(L-Arg)]–GA and –IA (see Tables 2 and 6) may be due to the small $\log K$ values and to the different experimental conditions required by the two techniques. The slightly larger standard deviations affecting GA and IA thermodynamic parameters result from the simultaneous determination of K and ΔH values. To be consistent the ΔH and ΔS values were refined by using the entries listed in the second column. The stability constants of the systems reported in Table 6 do show some sizeable differences; for example all the adducts with A = L-Arg are more stable than the analogous adducts with A = L-Ala. To have a more detailed description of the complexes we split the ΔG° value

Table 6. Stability constants and thermodynamic parameters for adduct formation (25 °C; pH 6.5 – 8.5; I = var.).[a]

System	log K		ΔG° [kJ mol^{-1}]	ΔH° [kJ mol^{-1}]	$T\Delta S^\circ$ [kJ mol^{-1}]
[Pt(bpm)(L-Arg)]$^{2+}$ – AMP	2.80(2)[b]	2.8(6)[d]	– 16.0	– 16.7(7)	– 0.7(7)
[Pt(bpm)(L-Ala)]$^{+}$ – AMP	2.14(2)[b]	2.15(9)[d]	– 12.2	– 12.4(8)	– 0.2(8)
[Pt(dpa)(en)]$^{2+}$ – AMP	2.58(2)[b]	2.6(1)[d]	– 14.8	– 8.8(7)	6.0(7)
[Pt(bpm)(en)]$^{2+}$ – AMP	2.39(4)[b]	2.4(6)[d]	– 13.7	– 10.8(5)	2.9(5)
[Pt(bpm)(L-Arg)]$^{2+}$ – GMP	2.96(4)[b]	2.95(9)[d]	– 16.8	– 17.0(7)	– 0.2(7)
[Pt(bpm)(L-Ala)]$^{+}$ – GMP	2.12(4)[b]	2.1(1)[d]	– 12.0	– 14.6(5)	– 2.6(5)
[Pt(dpa)(en)]$^{2+}$ – GMP	2.45(5)[b]	2.47(9)[d]	– 14.1	– 10.6(6)	3.5(6)
[Pt(bpm)(en)]$^{2+}$ – GMP	2.39(5)[b]	2.4(1)[d]	– 13.7	– 11.3(5)	2.4(5)
[Pt(bpm)(L-Arg)]$^{2+}$ – IA	2.29(1)[c]	2.01(4)[e]	– 11.4	– 33(1)	– 22(1)
[Pt(bpm)(L-Ala)]$^{+}$ – IA	1.84(2)[c]	1.81(9)[d]	– 10.3	– 29(1)	– 19(1)
[Pt(bpm)(L-Arg)]$^{2+}$ – GA	2.20(6)[c]	1.9(1)[e]	– 10.8	– 41(1)	– 30(1)
[Pt(bpm)(L-Ala)]$^{+}$ – GA	1.84(5)[c]	1.91(7)[d]	– 10.9	– 29(1)	– 18(1)

[a] Values in parentheses denote estimated standard deviations. [b] Determined by absorption spectroscopy. [c] Determined by ^{1}H NMR spectroscopy. [d] Checked by calorimetry. [e] Determined by calorimetry.

into enthalpic and entropic contributions. In fact, comparable stability constant values may result from significantly different enthalpic and entropic contributions. For instance, the formation of the adduct between four different methyl substituted ammonium cations and a water-soluble resorcarene is characterized by an almost identical ΔG° value, yet resulting from opposite enthalpic and entropic contributions.[43] The adducts of [Pt(phen)(en)] with GMP and IMP also exhibited opposite contributions of these parameters.[27]

Table 6 shows that all the adducts are enthalpically favored. The thermodynamic values indicate that the adduct formation is invariably driven by the enthalpic contribution irrespective of the molecules providing the donor atoms involved in the coordination to Pt^{II}, that is, L-Ala, L-Arg, or en, as well as of the species involved in the stacking, that is, AMP, GMP, IA, or GA. This is not surprising because experimental evidence does indicate that for the interaction of small molecules in water, this is the rule rather than the exception. In other words, it is the mutual attraction between the interacting particles rather than their desolvation that mainly drives the formation of the adduct. This clearly indicates that in all the complexes we are dealing with a "non-classical" hydrophobic effect.[26–28, 44–51] The data also show that the adduct is more rigidified when the guest molecule is IA or GA, negative ΔH° values of which are more than twice as large as the corresponding values for NMP, showing that stacking of a nucleotide, irrespective of the Pt^{II} complexes taken into consideration, results in a significant drop of the enthalpic contribution ($|\Delta H^\circ_{AR}| > |\Delta H^\circ_{NMP}|$ and $\Delta S^\circ_{AR} \ll \Delta S^\circ_{NMP}$).

There is an even more subtle aspect that deserves some comments. Regardless of the ligands involved in the primary coordination to Pt^{II}, the stability (ΔG°) of the adducts of **2** containing L-Arg is greater than that of the L-Ala-containing analogues. The greater stability of the L-Arg-containing adducts results from a difference in the enthalpic contribution between the L-Arg- and L-Ala-containing adducts. It has to be underlined that in the comparison between them any difference arising from factors that are difficult to be analyzed separately (e.g. the solvation of guests, solvation of the complexes) is factored out in the sense that we are considering differences ($\Delta\Delta G^\circ$ or $\Delta\Delta H^\circ$) only. The ΔH° contribution for **2**$\cdots$AR and **2**$\cdots$NMP is larger than that of the corresponding adducts with **1** (Table 6). This indicates that the electrostatic interaction between the guanidinium and carboxylate or phosphate groups as seen in Figure 6 is possible only for the L-Arg-containing systems and anchors the guests, thus rendering the stacking interaction more efficient. This in turn results in a more favorable enthalpic contribution.

The systems containing en show ΔH° values that are lower than those obtained for the analogous systems containing either L-Ala or L-Arg. This is to be related with the greater electron donor ability of en compared with L-Arg or L-Ala. An electron richer moiety (e.g. [Pt(bpm)(en)] as compared with [Pt(bpm)(L-Arg)]) is less prone to accept electrons from the donating moiety (GMP or AMP), which results in a weaker stacking interaction. This is seen from the ^{195}Pt NMR $\Delta\delta_{Pt}$ values as well as from the enthalpic values that are lower than those obtained for the [Pt(bpm)(A)] complexes.

Structures of adducts and structure – stability relationship as a basis of molecular recognition and self-organization

Crystal structure analysis of the isolated adducts, **3**, **5**, and **7** revealed that the Pt^{II} complexes as hosts bind with AR and NMP molecules as guests by $\pi-\pi$ interactions and various hydrogen bonds or electrostatic interactions. For example, the molecular structure of **3** shows how the Pt^{II}-complex **1** and IA are held together to form an adduct by stacking between the IA indole and bpm rings complemented by a hydrogen bond between the IA carboxylate and coordinated amino groups. In all the cases, the stacking between coordinated bpm and the aromatic ring of AR or NMP, which may be crucial for molecular association, and the hydrogen bonding contribute to stability and host – guest orientation of the resulting molecular assembly; $\pi-\pi$ stacking leads to formation of piles of aromatic rings, while hydrogen bonds connect the adducts to form an organized structure. The ^{1}H NMR spectra clearly indicate the presence of the stacking interaction within the adduct in dilute solution. The upfield shift due to the ring current effect is larger for the indole ring of IA than for the purine ring of AMP and GMP, which may reflect the energy of stacking. The thermodynamic parameters and ^{195}Pt NMR downfield shifts clearly show that the stacking is a bonding interaction with a negative ΔH° values. The presence of L-

Arg in the complexes caused further upfield shifts most probably due to the guanidinium–carboxylate or –phosphate hydrogen bonds, which are considered to fix interacting molecules in certain positions and increase the adduct stability. The ESI-MS spectrum of **4** gave the peak due to [Pt(bpm)(L-Arg)](IA)$^+$ (m/z_{obsd} 701.2) as confirmed by the isotope pattern, indicating that the adduct species is present in solution.

IA forms stable adducts with the Pt^{II} complexes probably due to its large indole ring with high electron density and hydrophobicity. This was further corroborated by ^{195}Pt NMR investigations, which revealed the largest electron density decrease of Pt^{II} in the present Pt^{II} complex–AR adducts. Since IA and NMP are to be regarded as electron donors in the stacked adducts, it is evident that a poorer donor (NMP) undergoes a less effective stacking, and this is reflected on less favorable enthalpic contribution (Table 6) as well as on the smaller $\Delta\delta$ values (Table 4). The downfield shifts of ^{195}Pt NMR may be interpreted as due to delocalization of electrons over the entire adduct structure. Intramolecular stacking such as in Cu(bpy)(AMP)[52–54] and Cu(bpy)(Trp)[29, 34, 55] has been established to increase the stability of the ternary complexes due to the bpy–adenine and bpy–indole stacking, respectively, as revealed by X-ray analysis. It is remarkable that the crystal structure of adduct **7** is constructed by the [Pt(bpm)(L-Arg)]···GMP units connected by the hydrogen bonds between the guanines and between the coordinated amino and phosphate groups, while the structures of IA- and GA-containing adducts, **3** and **5**, respectively, are essentially constructed by piles of stacked aromatic rings, and effective interactions, that is, the $\pi-\pi$ interactions in **3** and the $\pi-\pi$ interactions and guanidinium–carboxylate double hydrogen bonds in **5**, occur between adduct units, leading to self-organized assemblies. The information obtained from the present studies will be a fundamental step toward understanding biological molecular recognition in protein–protein, protein–DNA, and protein–ligand interactions and construction of functional molecular assemblies.

Experimental Section

Materials: AMP was purchased from Oriental Yeast, Ado from Kojin, GMP, CMP, and UMP from Yamasa Shoyu, $K_2[PtCl_4]$ from Tanaka Noble Metals, bpm from Lancaster, bpy from Wako, en, SA, GA (sodium salt), and dpa from Tokyo Kasei, and IA (potassium salt), phen, and amino acids (L-Arg, L-Lys, L-Ala, and Gly) from Nacalai Tesque. Deuterium oxide was obtained from Merck.

Spectral measurements: Absorption spectra were measured at room temperature with a Shimadzu UV-3101PC recording spectrophotometer. ^{1}H and ^{195}Pt NMR spectra were recorded at 23 °C with a Varian VXR-300S NMR spectrometer with *t*BuOH and $[Pt(en)_2]Cl_2$ as internal standards, respectively. Electro-spray ionization mass spectra (ESI-MS) were measured with a Perkin-Elmer Sciex API-300 mass spectrometer. All the samples were prepared by dissolving the complexes, organic carboxylates, and nucleotides in water or deuterium oxide. SA was dissolved in water containing an equivalent amount of NaOH.

[PtCl$_2$(bpm)]: bpm (0.32 g, 2 mmol) dissolved in MeOH (50 mL) was added to a solution of $[PtCl_2(dmso)_2]$[56] (0.85 g, 2 mmol) in water (100 mL), and the mixture was stirred overnight at room temperature. The precipitate was collected by filtration (0.84 g, 96%). Elemental analysis calcd (%) for $C_8H_6N_4Cl_2Pt\cdot0.5H_2O$ (433.16): C 22.18, H 1.63, N 12.93; found: C 22.30, H 1.48, N 12.89.

[PtCl$_2$(dpa)]: This was prepared in the manner described for [PtCl$_2$(bpm)] from $[PtCl_2(dmso)_2]$ (2.11 g, 5 mmol) and dpa (0.86 g, 5 mmol) to yield the title compound (2.0 g, 86%). Elemental analysis calcd (%) for $C_7H_{10}N_2Cl_2Pt$ (388.16): C 27.47, H 2.07, N 9.62; found: C 27.73, H 2.17, N 9.50.

[Pt(bpm)(L-Ala)]Cl (1): A solution of L-Ala (0.10 g, 1.5 mmol) and *t*BuOK (0.13 g, 1.5 mmol) in water (10 mL) was added to a suspension of [PtCl$_2$(bpm)] (0.43 g, 1 mmol) in 50% aq MeOH (50 mL), and the mixture was stirred at 70–80 °C until a clear solution was obtained. The solution was concentrated, and the residue was recrystallized twice from aq acetone to give the product as a yellow powder (75 mg, 15%). Elemental analysis calcd (%) for $C_{11}H_{12}N_5O_2ClPt\cdot H_2O$ (494.80): C 26.70, H 2.85, N 14.15; found: C 26.97, H 2.61, N 14.41.

[Pt(bpm)(L-Arg)]Cl$_2$ (2): This was prepared analogously from [PtCl$_2$(bpm)] (0.43 g, 1 mmol) and L-Arg (0.21 g, 1.2 mmol) without addition of *t*BuOK to yield yellow plates (0.11 g, 16%). Elemental analysis calcd (%) for $C_{14}H_{20}N_8O_2Cl_2Pt\cdot3H_2O$ (652.40): C 25.77, H 4.02, N 17.18; found: C 25.80, H 3.90, N 17.33.

[Pt(bpm)(L-Ala)](IA) (3): Complex **1** (72 mg, 0.15 mmol) and IA (38 mg, 0.18 mmol) were dissolved in 50% aq MeOH (20 mL), and the solution was stirred for 1 h and concentrated. Recrystallization from aq EtOH gave red plates (59 mg, 53%). Elemental analysis calcd (%) for $C_{21}H_{20}N_6O_4Pt\cdot7H_2O$ (741.61): C 34.01, H 4.62, N 11.33; found: C 34.14, H 4.37, N 11.49.

[Pt(bpm)(L-Arg)](IA)Cl (4): Complex **2** (0.13 g, 0.2 mmol) and IA (50 mg, 0.24 mmol) were dissolved in 50% aq MeOH (10 mL), and the solution was stirred for 1 h and concentrated. Recrystallization from acetone/MeOH gave a reddish brown powder (84 mg, 37%). Elemental analysis calcd (%) for $C_{24}H_{28}N_9O_4ClPt\cdot H_2O$ (755.09): C 38.18, H 4.00, N 16.69; found: C 38.36, H 4.08, N 16.76.

[Pt(bpm)(L-Arg)](GA)Cl (5): Complex **2** (32 mg, 0.05 mmol) and the sodium salt of GA (11 mg, 0.05 mmol) were dissolved in 50% aq MeOH (10 mL), and the solution was stirred for 1 h and concentrated. Recrystallization from aq acetone gave orange needles (14 mg, 37%). Elemental analysis calcd (%) for $C_{21}H_{25}N_8O_6ClPt\cdot2H_2O$ (752.04): C 33.54, H 3.89, N 14.90; found: C 33.42, H 3.82, N 15.18.

[Pt(bpm)(L-Ala)](GA) (6): This was prepared in the manner described for **5** from **1** (24 mg, 0.05 mmol) and GA (11 mg, 0.05 mmol) to yield orange needles (12 mg, 39%). Elemental analysis calcd (%) for $C_{18}H_{17}N_5O_6Pt\cdot H_2O$ (612.46): C 35.30, H 3.13, N 11.43; found: C 35.02, H 2.93, N 11.56.

[Pt(bpm)(L-Arg)](GMP) (7): A solution of complex **2** (64 mg, 0.1 mmol) and GMP (disodium salt, 52 mg, 0.1 mmol) in water (5 mL) was stirred overnight, and the precipitate was filtered and recrystallized from water to give yellow plates (40 mg, 39%). Elemental analysis calcd (%) for $C_{24}H_{32}N_{13}O_{10}PPt\cdot5H_2O$ (978.73): C 29.45, H 4.33, N 18.60; found: C 29.21, H 4.37, N 18.46.

[Pt(bpm)(Gly)]Cl (8): This was prepared in a manner similar to that for **1** to yield a pale yellow powder (82 mg, 17%). Elemental analysis calcd (%) for $C_{10}H_{10}N_5O_2ClPt\cdot H_2O$ (480.77): C 24.98, H 2.50, N 14.57; found: C 25.05, H 2.34, N 14.71.

[Pt(bpm)(en)]Cl$_2$ (9): bpm (0.17 g, 1.1 mmol) dissolved in a small amount of water was added to a suspension of [PtCl$_2$(en)] (0.33 g, 1.0 mmol) in water (30 mL), and the mixture was stirred for 2 h at 80 °C, filtered, concentrated to a small volume, and mixed with MeOH to give an orange powder (90 mg, 18%). Elemental analysis calcd (%) for $C_{10}H_{14}N_6Cl_2Pt\cdot2H_2O$ (520.28): C 23.09, H 3.49, N, 16.15; found: C 22.80, H 3.23, N 15.97.

[Pt(bpy)(L-Arg)]Cl$_2$ (10): This was prepared according to the procedure for **2** to yield a yellow powder (0.13 g, 16%). Elemental analysis calcd (%) for $C_{16}H_{22}N_6O_2Cl_2Pt\cdot2H_2O$ (632.41): C 30.39, H 4.14, N 13.29; found: C 30.24, H 3.92, N 13.22.

[Pt(bpy)(L-Lys)](ClO$_4$)$_2$ (11): [PtCl$_2$(bpy)] (85 mg, 0.2 mmol), L-Lys·HCl (37 mg, 0.2 mmol), and $NaHCO_3$ (30 mg, 0.2 mmol) were mixed in aq EtOH and stirred at 70 °C, when a clear yellow solution was obtained. The solution was further stirred for 2–3 h at 70 °C, filtered, and concentrated to give a precipitate, which was removed by filtration. The filtrate was mixed with a small volume of aq $NaClO_4$ (ca. 5 M) and kept overnight in a refrigerator after concentration to yield a yellow powder (70 mg, 47%).

Elemental analysis calcd (%) for $C_{16}H_{22}N_4O_{10}Cl_2Pt \cdot 2H_2O$ (732.39): C 26.24, H 3.58, N 7.65; found: C 26.39, H 3.15, N 7.49.

Caution! Perchlorates may be explosive and should be handled with caution.

[Pt(bpy)(L-Ala)]ClO_4 (12): $Na_2CO_3 \cdot H_2O$ (62 mg, 0.5 mmol) dissolved in a small volume of water was added to a suspension of [$PtCl_2$(bpy)] (0.42 g, 1.0 mmol) and L-Ala (89 mg, 1.0 mmol) in aq MeOH, and the mixture was stirred for 3 h at 80 °C, filtered, and concentrated. The residue was mixed with aq $NaClO_4$ (2.5 equiv) and a small volume of EtOH and kept in a refrigerator to yield a yellow powder (0.12 g, 22%). Elemental analysis calcd (%) for $C_{13}H_{14}N_3O_6ClPt$ (538.80): C 28.98, H 2.62, N 7.80; found: C 29.19, H 2.43, N 7.69.

[Pt(dpa)(en)]Cl_2 (13): A solution of en (0.78 g, 1.3 mmol) in a small volume of water was added to a suspension of [$PtCl_2$(dpa)] (0.44 g, 1.0 mmol) in water (30 mL), and the mixture was stirred for 2 h at 80 °C and filtered. The filtrate was concentrated to a small volume (5 mL), when a pale yellow precipitate was formed. Recrystallization from MeOH gave pale yellow needles (0.33 g, 60%). Elemental analysis calcd (%) for $C_{12}H_{17}N_5Cl_2Pt \cdot 3H_2O$ (551.33): C 26.14, H 4.21, N 12.70; Found: C 26.40, H 4.10, N 12.73.

[Pt(bpy)(en)]Cl_2 and [Pt(phen)(en)]Cl_2 were prepared according to the literature.[57]

Calorimetric measurements: Thermogravimetric data were obtained by means of a Perkin–Elmer thermal analyzer TGS-2. The measurements were carried out by heating samples of about 3–4 mg mass at 10 K min^{-1} in air from room temperature up to a final temperature of 900 °C. The calorimetric runs were performed under isoperibol conditions. The measurements were performed with a Tronac 450 isoperibol calorimeter equipped with a 4 mL dewar cell. This calorimeter measured the temperature changes following the addition of a titrant through a precision thermistor which generated a voltage output. This output was converted into a heat quantity by a precision heater.[58] The calorimetric apparatus was calibrated by titrating 2-amino-2-hydroxymethyl-1,3-propanediol (tris) with HCl.[59] As recommended, the dewar was calibrated beforehand to ensure that the volume increase resulting from addition of the titrant did not cause an increase in the heat leakage constant of the calorimetric vessel. For the experiments described here the volume upper limit was found to be 3.4 mL. Consequently the amount of titrant added was never allowed to exceed 0.3 mL. Usually a solution of AMP or GMP (0.06–0.07 M) or a solution of IA or GA (0.1 M) was added to 3 mL of a 3–5 mM solution of an appropriate platinum complex. Although it would have been highly desirable to have higher titrant concentrations to maximize heat effects, these concentrations were kept below the upper limit to avoid problems connected with nucleotide self-stacking.[60, 61] Blank experiments (see below) were carried out for evaluation of heat contributions arising from association/dissociation of the nucleotide. IA and GA solutions employed as titrants were always freshly prepared. For each system 3–5 different independent titrations were performed. In all cases the titration data, corrected for all non-chemical energy terms determined by separate experiments, were refined simultaneously using the computer program DOEC,[62] which minimizes the function $U = \Sigma_j w_j (Q_{i,calcd} - Q_{j,exptl})^2$. Here Q_j is the heat of reaction at the jth point and is related to ΔH by $-Q_j = \Sigma_i \Delta H_i \delta n_{i,j}$, where δn_i and ΔH_i are the number of moles and the enthalpy of the ith species (one in the present case), respectively, for obtaining the final ΔH values.

X-ray structure determinations: Diffraction data for **2**, **3**, and **5** were collected at 295 K with a Rigaku AFC-7R four-circle automated diffractometer with graphite-monochromated $Mo_{K\alpha}$ radiation ($\lambda = 0.71073$ Å) using a rotating anode generator. Crystals suitable for X-ray analysis were obtained by recrystallization and mounted on a glass fiber. Accurate cell dimensions were determined by least-squares refinement using 25 carefully centered reflections with appropriate intensities. Intensity data were collected by the ω-2θ scan technique with the scan rate of 16° min^{-1}(ω). The reflection intensities were monitored by three standard reflections at every 150 reflections, and the decays of intensities for all crystals were within 2%. All the data were corrected for both Lorentz and polarization effects, and empirical absorption corrections were applied by using the DIFABS program.[63] Diffraction data of **7** were collected at 295 K with a Rigaku/MSC Mercury diffractometer with graphite monochromated $Mo_{K\alpha}$ radiation for a crystal mounted on a glass fiber. A total of 720 oscillation

Table 7. Crystallographic data.

	2	**3**	**5**	**7**
formula	$C_{14}H_{26}N_8O_5Cl_2Pt$	$C_{21}H_{34}N_6O_{11}Pt$	$C_{42}H_{58}N_{16}O_{16}Cl_2Pt_2$	$C_{24}H_{42}N_{13}O_{15}PPt$
F_w	652.41	741.62	1504.1	987.74
crystal color, habit	yellow, plate	red, prismatic	orange, needle	yellow, plate
crystal dimensions [mm]	0.30 × 0.20 × 0.10	0.20 × 0.20 × 0.20	0.50 × 0.20 × 0.05	0.50 × 0.20 × 0.03
crystal system	orthorhombic	orthorhombic	orthorhombic	monoclinic
lattice parameters				
a [Å]	11.262(2)	17.412(3)	13.882(3)	8.828(2)
b [Å]	18.181(2)	22.759(4)	29.917(2)	11.060(2)
c [Å]	11.004(2)	7.017(2)	12.704(2)	18.214(3)
β [°]				94.537(10)
V [Å^3]	2253.0(5)	2780(1)	5276(1)	1772.9(6)
space group	$P2_12_12_1$	$P2_12_12_1$	$P2_12_12_1$	$P2_1$
Z	4	4	4	2
ρ_{calcd} [g cm^{-3}]	1.923	1.771	1.893	1.833
F(000)	1272	1472	2960	980
μ ($Mo_{K\alpha}$) [cm^{-1}]	64.82	50.92	54.61	40.74
$2\theta_{max}$ [°]	59.99	55.01	50.00	54.96
absorption correction	DIFABS[a]	DIFABS[a]	DIFABS[a]	numerical
transmission factors	0.3046–0.5230	0.2962–0.3612	0.6445–0.7611	
no. measd refls	3701	3648	5197	8300
no. independent refls	3675	3618	5165	7960
no. refls Included in refinement	3675	3618	5165	7949
no. variables	273	434	704	488
program of structure solution	SIR92[b]	SIR92[b]	MITHRIL90[c]	MITHRIL90[c]
R; R_w[d]	0.088; 0.133	0.057; 0.089	0.069; 0.092	0.118; 0.204
$R1$[e]	0.047	0.034	0.037	0.077
no. refls to calcd $R1$	2761	2818	2932	6393
p Factor	0.078	0.044	0.026	0.074
residual el. density [e Å^{-3}]	3.35	1.00	1.09	1.95

[a] DIFABS.[44] [b] SIR92.[45] [c] MITHRIL90.[46] [d] $R = \Sigma||F_o| - |F_c||/\Sigma|F_o|$, $R_w = \{\Sigma\omega(|F_o| - |F_c|)^2/\Sigma\omega F_o^2\}^{1/2}$; $\omega = 1/\sigma^2(F_o) = \{\sigma_c^2(F_o) + p^2/4F_o^2\}^{-1}$. [e] $R_1 = \Sigma||F_o| - |F_c||/\Sigma|F_o|$ for $I > 2\sigma(I)$ data.

images were collected using ω scans from -70.0 to 100.0° in 0.50° steps, at $\chi = 45.0^\circ$ and $\phi = 0.0$ and 90.0°. These data were collected and processed using the CrystalClear program and corrected for Lorentz and polarization effects, numerical absorption corrections being applied. Crystal data and experimental details of the data collection for all the complexes analyzed are summarized in Table 7.

The structures were solved by the direct method using SIR92[64] or MITHRIL90[65] and expanded by Fourier techniques using the DIRDIF program.[66] The non-hydrogen atoms were refined anisotropically against $|F^2|$ by full-matrix least-squares calculations using all the reflection data. Atomic scattering factors[67] and anomalous dispersion terms[68] were taken from the literature. Hydrogen atoms for all structures were located at the calculated positions with $d(\mathrm{C-H}) = 0.95$ Å except for water molecules and hydroxyl groups of **5**, and all hydrogen atoms were not refined. All the calculations were performed by using the teXan program package.[69]

CCDC-201005 (**2**), -201006 (**3**), -201007 (**5**), -201008 (**7**) contain the supplementary crystallographic data for this paper. These data can be obtained free of charge via www.ccdc.cam.ac.uk/conts/retrieving.html (or from the Cambridge Crystallographic Data Centre, 12 Union Road, Cambridge CB21EZ, UK; fax: (+44) 1223-336-033; or deposit@ccdc.cam.uk).

Acknowledgement

We thank Professors Kazuyuki Tatsumi (Nagoya University) and Yoshihito Watanabe (Nagoya University) for the support of X-ray diffraction measurements. We gratefully acknowledge the financial support of this work by the Grants-in-Aid for Scientific Research (Nos. 09304062 and 13440202 to O.Y.) from the Ministry of Education, Culture, Sports, Science, and Technology of Japan. Partial support by MIUR ("Biomedicine" Cluster 04-Project 17 and PRIN MM 03108222-003) to G.A. is gratefully acknowledged. This work was partly supported by the Kansai University Grant-in-Aid for Faculty Joint Research Program, 2002.

[1] See for example: a) E. Frieden, *J. Chem. Educ.* **1975**, *52*, 754; b) A. R. Fresht, *Structure and Mechanism in Protein Science*, Freeman, New York, **1999**; c) S. K. Burley, G. A. Petsko, *Adv. Protein Chem.* **1988**, *39*, 125; d) B. Alberts, D. Bray, J. Lewis, M. Raff, K. Roberts, J. D. Watson, *Molecular Biology of the Cell*, 3rd ed., Garland, New York, **1994**, pp. 89–138.
[2] L. Serrano, M. Bycroft, A. R. Fersht, *J. Mol. Biol.* **1991**, *218*, 465.
[3] C. A. Hunter, J. Singh, J. M. Thornton, *J. Mol. Biol.* **1991**, *218*, 837.
[4] T. E. Creighton, *Proteins*: *Structure and Molecular Properties*, 2nd ed., Freeman, New York, **1993**.
[5] C. Branden, J. Tooze, *Introduction to Protein Structure*, 2nd ed., Garland Publishing, New York, **1998**.
[6] W. Saenger, *Principles of Nucleic Acid Structure*, Springer, Heidelberg, **1984**.
[7] See for example: a) H. B. Gray, W. R. Ellis, Jr. in *Bioinorganic Chemistry* (Eds.: I. Bertini, H. B. Gray, S. J. Lippard, J. S. Valentine), University Science Books, Mill Valley, **1994**, pp. 315–363; b) H. Pelletier, J. Kraut, *Science* **1992**, *258*, 1748; c) L. Chen, R. Durley, F. S. Machews, V. L. Davidson, *Science* **1994**, *264*, 86.
[8] M. Nishio, M. Hirota, Y. Umezawa, *The CH/π Interactions*, Wiley-VCH, New York, **1998**.
[9] M. Perutz, *Philos. Trans. R. Soc. London Ser. A* **1993**, *345*, 105.
[10] D. A. Dougherty, *Science* **1996**, *271*, 163.
[11] C. J. Ma, D. A. Dougherty, *Chem. Rev.* **1997**, *97*, 1303.
[12] J. P. Gallivan, D. A. Dougherty, *Proc. Natl. Acad. Sci. USA* **1999**, *96*, 9459.
[13] N. Zacharias, D. A. Dougherty, *Trends Pharmacol. Sci.* **2002**, *23*, 281.
[14] For reviews, see for example: a) J.-M. Lehn, *Science* **2002**, *295*, 2400, and references therein; b) J.-P. Sauvage, *Perspective in Supramolecular Chemistry*, *Vol. 5*, Wiley, New York, **1999**; c) M. Fujita, *Struct. Bonding (Berlin)* **2000**, *96*, 177.
[15] O. Yamauchi, A. Odani, M. Takani, *J. Chem. Soc. Dalton Trans.* **2002**, 3411.
[16] K. W. Jennette, S. J. Lippard, G. A. Vassiliades, W. R. Bauer, *Proc. Natl. Acad. Sci. USA* **1974**, *71*, 3839.
[17] S. J. Lippard, P. J. Bond, K. C. Wu, W. R. Bauer, *Science* **1976**, *194*, 726.
[18] J. K. Barton, S. J. Lippard in *Nucleic Acid-Metal ion Interactions* (Ed.: T. G. Spiro), Wiley, New York, **1980**, pp. 31–113.
[19] J. K. Barton, A. T. Danshefsky, J. M. Goldberg, *J. Am. Chem. Soc.* **1984**, *106*, 2172.
[20] J. K. Barton, *Science* **1986**, *233*, 727.
[21] A. M. Pyle, J. K. Barton, *Prog. Inorg. Chem.* **1990**, *38*, 413.
[22] J. K. Barton in *Bioinorganic Chemistry* (Eds.: I. Bertini, H. B. Gray, S. J. Lippard, J. S. Valentine), University Science Book, Mill Valley, **1994**, p. 455.
[23] B. Nordén, P. Lincoln, B. Åkerman, E. Tuite, *Met. Ions Biol. Syst.* **1996**, *33*, 177.
[24] The following abbreviations were used: bpy, 2,2′-bipyridine; bpm, 2,2′-bipyrimidine; dpa, di(2-pyridylmethyl)amine; phen, 1,10-phenanthroline; L-Arg, L-arginine; L-Lys, L-lysine; L-Asn, L-asparginate; L-Gln, L-glutaminate; L-Ala, L-alaninate; Gly, glycinate; en, ethylenediamine; IA, indole-3-acetate; GA, gentisate; SA, salicylate; NMP, nucleotide 5′-monophosphate; AMP, adenosine 5′-monophosphate; GMP, guanosine 5′-monophosphate; CMP, cytidine 5′-monophosphate; UMP, uridine 5′-monophosphate; Ado, adenosine.
[25] O. Yamauchi, A. Odani, R. Shimata, Y. Kosaka, *Inorg. Chem.* **1986**, *25*, 3337.
[26] A. Odani, R. Shimata, H. Masuda, O. Yamauchi, *Inorg. Chem.* **1991**, *30*, 2133.
[27] A. Odani, H. Masuda, O. Yamauchi, S. Ishiguro, *Inorg. Chem.* **1991**, *30*, 4484.
[28] A. Odani, T. Sekiguchi, H. Okada, S. Ishiguro, O. Yamauchi, *Bull. Chem. Soc. Jpn.* **1995**, *68*, 2093.
[29] O. Yamauchi, A. Odani, H. Masuda, H. Sigel, *Met. Ions Biol. Syst.* **1996**, *32*, 207.
[30] Y.-S. Wong, J. S. Lippard, *J. Chem. Soc. Chem. Commun.* **1977**, 824.
[31] H. Masuda, O. Yamauchi, *Inorg. Chim. Acta* **1987**, *136*, L29.
[32] G. Brookes, L. D. Pettit, *J. Chem. Soc. Dalton Trans.* **1977**, 1918.
[33] B. E. Fischer, H. Sigel, *J. Am. Chem. Soc.* **1980**, *102*, 2998.
[34] O. Yamauchi, A. Odani, *J. Am. Chem. Soc.* **1985**, *107*, 5938.
[35] O. Yamauchi, A. Odani, H. Masuda, *Inorg. Chim. Acta* **1992**, *198–200*, 749.
[36] H. Masuda, A. Odani, T. Yamazaki, T. Yajima, O. Yamauchi, *Inorg. Chem.* **1993**, *32*, 1111.
[37] O. Yamauchi, A. Odani, S. Hirota, *Bull. Chem. Soc. Jpn.* **2001**, *74*, 1525.
[38] D. M. Roundhill in *Comprehensive Coordination Chemistry*, *Vol. 5* (Eds.: G. Wilkinson, R. D. Gillard, J. A. McCleverty), Pergamon, Oxford, **1987**, Chapter 52, p. 351.
[39] G. Laughlan, A. I. H. Murchie, D. G. Norman, M. H. Moore, P. C. E. Moody, D. M. J. Lilley, B. Luisi, *Science* **1994**, *265*, 520.
[40] M. P. Horvath, S. C. Schultz, *J. Mol. Biol.* **2001**, *310*, 367.
[41] F. A. Bovey, *Nuclear Magnetic Resonance Spectroscopy*, Academic Press, New York, **1969**.
[42] C. W. Haigh, R. B. Mallion, *Org. Magn. Reson.* **1972**, *4*, 203.
[43] G. Arena, A. Contino, T. Fujimoto, D. Sciotto, Y. Aoyama, *Supramol. Chem.* **1999**, *11*, 279.
[44] R. Corradini, A. Dossena, G. Impellizzeri, G. Maccarrone, R. Marchelli, E. Rizzarelli, G. Sartor, G. Vecchio, *J. Am. Chem. Soc.* **1994**, *116*, 10267.
[45] G. Arena, R. Calì, V. Cucinotta, S. Musumeci, E. Rizzarelli, S. Sammartano, *J. Chem. Soc. Dalton Trans.* **1983**, 1271.
[46] G. Arena, *Sunner Memorial Award Lecture*, *Proceedings of the 44th Calorimetry Conference*, Oak Ridge, Tennessee, USA, August 2, **1989**, p. 84.
[47] D. B. Smithrud, T. B. Wyman, F. J. Diederich, *J. Am. Chem. Soc.* **1991**, *113*, 5420.
[48] M. A. Petti, T. J. Sheppod, R. E. Barrans, D. A. Dougherty, *J. Am. Chem. Soc.* **1988**, *110*, 6825.
[49] R. L. Biltonen, N. Langerman, *Methods Enzymol.* **1979**, *61*, 287.
[50] G. Arena, A. Casnati, A. Contino, G. G. Lombardo, D. Sciotto, R. Ungaro, *Chem. Eur. J.* **1999**, *5*, 738.
[51] G. Arena, A. Casnati, A. Contino, F. G. Gulino, D. Sciotto, R. Ungaro, *J. Chem. Soc. Perkin Trans. 2* **2000**, 419.
[52] K. Aoki, *J. Am. Chem. Soc.* **1978**, *100*, 7106.
[53] P. R. Mitchell, B. Prijs, H. Sigel, *Helv. Chim. Acta* **1979**, *62*, 1723.

[54] K. Aoki, *Met. Ions Biol. Syst.* **1996**, *32*, 91.
[55] H. Masuda, T. Sugimori, A. Odani, O. Yamauchi, *Inorg. Chim. Acta* **1991**, *180*, 73.
[56] J. H. Price, A. N. Williamson, R. F. Schramm, B. B. Wayland, *Inorg. Chem.* **1972**, *11*, 1280.
[57] W. D. McFadyen, L. P. G. Wakelin, I. A. G. Roos, V. A. Leopold, *Med. Chem.* **1985**, *28*, 1113.
[58] J. J. Christensen, J. Ruckmann, D. J. Eatought, R. M. Izatt, *Thermochim. Acta* **1972**, *3*, 219.
[59] I. Grenthe, H. Otsand, O. Ginstrupp, *Acta Chem. Scand.* **1970**, *24*, 1067.
[60] M. P. Heyn, R. Bretz, *Biophys. Chem.* **1975**, *3*, 35.
[61] K. H. Scheller, F. Hofstetter, P. R. Mitchell, B. Prijs, H. Sigel, *J. Am. Chem. Soc.* **1981**, *103*, 247.
[62] C. Rigano, E. Rizzarelli, S. Sammartano, *Thermochim. Acta* **1979**, *33*, 211.
[63] N. Walker, D. Stuart, *Acta Crystallogr. Sect. A* **1983**, *39*, 158.
[64] A. Altomare, M. C. Burla, M. Camalli, M. Cascarano, C. Giacovazzo, A. Guagliardi, G. Polidori, *J. Appl. Crystallogr.* **1994**, *27*, 435.
[65] C. J. Gilmore, MITHRIL, Integrated Direct Methods Computer Program, University of Glasgow, Scotland, **1990**.
[66] P. T. Beurskens, G. Admiraal, G. Beurskens, W. P. Bosman, R. de Gelder, R. Israel, J. M. M. Smits, DIRDIF-94 program system, Technical Report of the Crystallography Laboratory, University of Nijmegen (The Netherlands), **1994**.
[67] D. T. Cromer, J. T. Waber, *International Tables for X-Ray Crystallography*, *Vol. IV*, Kynoch, Birmingham, **1974**.
[68] D. C. Creagh, W. J. McAuley in *International Tables for Crystallography*, *Vol. C* (Ed.: A. J. C. Wilson), Kluwer Academic, Boston, **1992**, pp. 219 – 222.
[69] Crystal Structure Analysis Package, Molecular Structure Corporation, **1985** and **1999**.

Received: January 11, 2003 [F4728]

